

Combining reconstruction and edge detection in computed tomography

Jürgen Friel¹, Simon Göppel², Markus Haltmeier²

¹Department of Computer Science and Mathematics, OTH Regensburg

²Department of Mathematics, University of Innsbruck

`juergen.friel@oth-regensburg.de`

Abstract

We present two methods that combine image reconstruction and edge detection in computed tomography (CT) scans. Our first method is as an extension of the prominent filtered backprojection algorithm. In our second method we employ ℓ^1 -regularization for stable calculation of the gradient. As opposed to the first method, we show that this approach is able to compensate for undersampled CT data.

1 Introduction

Detection of edges in computed tomography (CT) scans is a challenging task because the underlying image reconstruction problem is ill-posed and, hence, even small errors in the x-ray measurements may lead to huge reconstruction errors that have to be compensated by the edge detection algorithms, cf. [1]. This task becomes even more challenging, when the CT scans are generated from a small number of x-ray measurements, as it is the case, e.g., in digital breast tomosynthesis or dental CT, where the x-ray measurements can be taken only from a small number of views in a limited angular range. In such situations, classical reconstruction algorithms may generate characteristic reconstruction artifacts (in

addition to noise amplification) and, thus, substantially degrade the image quality, cf. [2]. Performing edge detection after image reconstruction, can therefore lead to unreliable edge maps. In this article we present two methods, that allow for a stable reconstruction of edges directly from CT data and, thus, stabilizes edge detection in CT images. In this work, we focus on stable reconstruction of the gradient of a CT scan, because it is the main ingredient in most prominent edge detection algorithms, such as the Canny algorithm, cf. [3].

In what follows, we model CT scans as functions $f : \mathbb{R}^2 \rightarrow \mathbb{R}$ and the corresponding CT data by the Radon transform of f , which is defined as (cf. [1])

$$\mathcal{R}f(\varphi, s) := \int_{\mathbb{R}} f(s\theta(\varphi) + t\theta^\perp(\varphi)) dt, \quad (1)$$

where $\theta(\varphi) = (\cos(\varphi), \sin(\varphi))^\top$ and $\theta^\perp(\varphi) = (-\sin(\varphi), \cos(\varphi))^\top$. Here, the value $\mathcal{R}f(\varphi, s)$ represents one x-ray measurement along the x-ray path that is given by the line $L(\varphi, s) = \{s\theta(\varphi) + t\theta^\perp(\varphi) : t \in \mathbb{R}\} = \{x \in \mathbb{R}^2 : \langle x, \theta(\varphi) \rangle = s\}$, where $\varphi \in [0, \pi)$ and $s \in \mathbb{R}$.

We will present two methods for stable reconstruction of the gradient of the smooth function $f_\varepsilon := f * g_\varepsilon$,

where

$$g_\varepsilon(x) := \frac{1}{2\pi\varepsilon^2} \exp\left(-\frac{\|x\|^2}{2\varepsilon^2}\right), \quad \varepsilon > 0. \quad (2)$$

First, we derive a method that is of the same type as the famous filtered backprojection algorithm (FBP). This method follows the spirit of [4] and yields good results whenever the CT data is well sampled [5]. In our second approach, we employ ideas from compressed sensing and propose to use sparse regularization for the reconstruction of the image gradient. We show that this method leads to a more robust edge detection, especially when the data is not sampled properly.

2 Materials and methods

2.1 Method 1: An FBP-type approach for calculating the gradient

In order to calculate the smoothed partial derivatives

$$\frac{\partial f_\varepsilon}{\partial x_j} = \frac{\partial}{\partial x_j}(f * g_\varepsilon) = f * \frac{\partial g_\varepsilon}{\partial x_j}, \quad (3)$$

directly from CT data, we use the well-known relations between the Radon transform, convolutions and derivatives (cf. [1]) and obtain the following result.

Lemma 2.1 *Let the Gaussian g_ε be defined by (2). Then, we have for $j \in \{1, 2\}$:*

$$\mathcal{R} \left[f * \frac{\partial g_\varepsilon}{\partial x_j} \right] (\varphi, s) = [\mathcal{R}f *_s G_{\varepsilon,j}] (\varphi, s), \quad (4)$$

where $*_s$ denotes the convolution with respect to the second variable s , and

$$G_{\varepsilon,j}(\varphi, s) := -\frac{\theta_j(\varphi)}{\varepsilon^3 \sqrt{2\pi}} \cdot s \cdot \exp\left(-\frac{s^2}{2\varepsilon^2}\right) \quad (5)$$

with $(\varphi, s) \in [0, \pi) \times \mathbb{R}$ and $\theta_1(\varphi) := \cos(\varphi)$, $\theta_2(\varphi) := \sin(\varphi)$.

Lemma 2.1 shows that the partial derivatives (3) can be obtained by applying the inverse Radon transform \mathcal{R}^{-1} to the preprocessed data (4), i.e.,

$$\frac{\partial f_\varepsilon}{\partial x_j} = \mathcal{R}^{-1} [\mathcal{R}f *_s G_{\varepsilon,j}]. \quad (6)$$

Since the FBP algorithm is a regularized implementation of \mathcal{R}^{-1} (cf. [1]), a standard toolbox implementation could be used in practice to obtain ∇f_ε .

Since the inverse Radon transform is given by $\mathcal{R}^{-1} = \mathcal{B} \circ P$, where P is a filtering (convolution) operator and \mathcal{B} is the so-called backprojection operator (cf. [1]), the filtering by P can be combined with the filtering in (6). In this way, we obtain a reconstruction formula of FBP-type for the derivatives (6), that is stated in the following theorem.

Theorem 2.2 *Let $W_{\varepsilon,j}$ be the function of two variables (φ, s) which is defined in the*

Fourier domain by

$$\widehat{W}_{\varepsilon,j}(\varphi, \omega) := \frac{1}{4\pi} \cdot \theta_j(\varphi) \cdot i \cdot \omega \cdot |\omega| \cdot \exp\left(\frac{-\varepsilon^2 \omega^2}{2}\right), \quad (7)$$

where $\widehat{W}_{\varepsilon,j}$ denotes the 1D-Fourier transform of $W_{\varepsilon,j}$ with respect to the s -variable and $i \in \mathbb{C}$ is the imaginary unit. Then,

$$\frac{\partial f_\varepsilon}{\partial x_j} = \mathcal{B}(\mathcal{R}f *_s W_{\varepsilon,j}), \quad (8)$$

where \mathcal{B} is the backprojection operator for the Radon transform (cf. [1]).

The proof of Theorem 2.2 follows from (4) together with the convolution theorem for the Fourier transform and Theorem II.2.1 in [1]. It shows that the derivatives (3) can be calculated using a FBP-algorithm with angle-dependent filters that are given by (7).

Remark 2.3 *The accuracy of the presented method (given by (6) and (8)) will strongly depend on the sampling of the Radon transform, cf. [1]. If the CT data does not satisfy the sampling requirements, e.g., when the angles are sampled rather sparsely, the algorithm will produce artifacts which can substantially degrade the performance of edge detection.*

2.2 Method 2: Gradient calculation using ℓ^1 -regularization

In order to account for the negative effects of (possible) undersampling of CT data, we propose to replace \mathcal{R}^{-1} in (6) by a regularization method for \mathcal{R}^{-1} that is able to deal with undersampled data. From the theory of compressed sensing it is well known that sparsity can help to overcome the classical Shannon sampling paradigm, [6]. As we are interested in recovering gradients of images, which only have large values around edges, we aim at enforcing sparsity of image gradients. Thus, we calculate the derivatives (3) approximately via (cf. [6]):

$$\mathbf{f}_{\lambda,\varepsilon}^{(j)} = \arg \min_{\mathbf{f}} \|\mathbf{R}\mathbf{f} - \mathbf{y} * G_{\varepsilon,j}\|_2^2 + \lambda \|\mathbf{f}\|_1, \quad (9)$$

where $\lambda > 0$ is regularization parameter. Note that in (9) the bold face symbols denote the discretized versions of the corresponding continuous objects.

3 Results

We implemented the methods 1 and 2 in Matlab and tested them on the x-ray CT data of a lotus root, cf. [7]. In our experiments we converted the fan-beam data to a parallel-beam data using Matlab function `fan2para` and downsampled this data in order to simulate angular undersampling. Thereby, we used 738 equispaced samples in the s -variable and 36 evenly distributed angles in $[0, \pi)$. For our implementations, we used the Matlab functions `radon` and `iradon` as numerical realizations of the Radon transform, the inverse Radon transform and the backprojection operator. For the minimization of the ℓ^1 -functional (9), we implemented the iterative soft thresholding algorithm, cf. [8].

The CT data and the corresponding FBP reconstruction are shown in Fig. 1(a) and 1(d). It can be clearly observed that the FBP reconstruction contains many undersampling artifacts (streaks) that could complicate the detection of edges in that image. Hence, we calculated the gradient directly from CT data using the methods 1 and 2, where we chose the parameters based on visual inspection of edge detection results. These are given in the caption of Fig. 1.

In Fig. 1(b) and 1(e) one can see that the Gaussian smoothing cannot compensate for the undersampling artifacts and, thus, many edges in the edge map are not coming from actual image features. However, the ℓ^1 -regularization successfully reduces the number of artifacts and detects the edges more reliably, as can be seen in Fig. 1(c) and 1(f). In other experiments we also observed that the method 2 outperforms the method 1 whenever the CT data was not sampled properly. For dense angular sampling, we found that both methods produce similar edge detection results.

4 Discussion

We presented two methods for calculating the gradient of a CT scan directly from CT data. As our first method, we introduced is a variant of the filtered backprojection algorithm and explained two different ways for its implementation. As our second approach, we introduced a sparsity based gradient recovery from CT data and showed in numerical experiments that this method is able to account for data undersampling and to provide more reliable edge

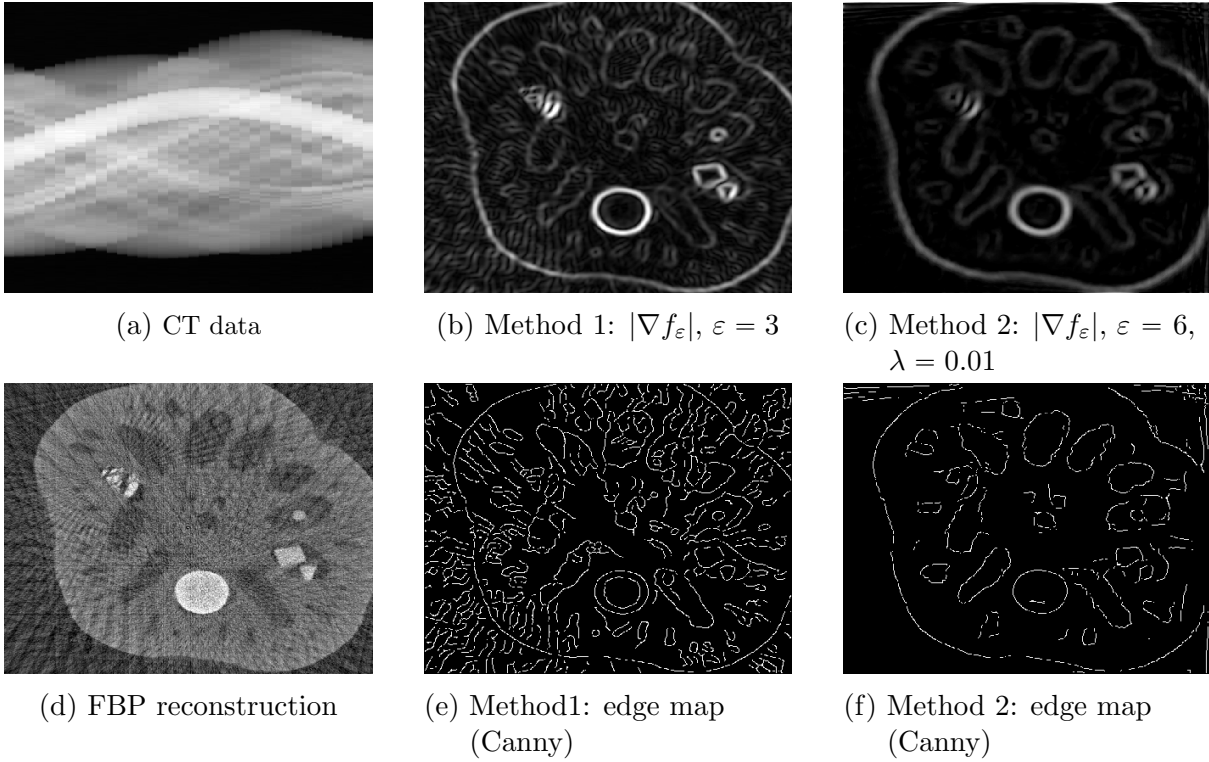


Figure 1: Rebinned CT data of a lotus root (a) and the corresponding FBP reconstruction (d) from an angular range given by $[0, \pi)$ and 36 evenly distributed angles, cf. [7]. The magnitude of the gradient $|\nabla f_\varepsilon|$, in (b) and (c), and the corresponding edge detection results using the Canny algorithm, see (e) and (f).

detection results. Moreover, the second approach provides more flexibility and can be more easily applied to different scanning geometries.

5 Acknowledgement

The contribution by S. G. is part of a project that has received funding from the European Union’s Horizon 2020 research and innovation programme under the Marie Skłodowska-Curie grant agreement No 847476. The views and opinions expressed herein do not necessarily reflect those of the European Commission.

References

- [1] Natterer F. The mathematics of computerized tomography. Stuttgart: B. G. Teubner; 1986.
- [2] Friel J, Quinto ET. Characterization and reduction of artifacts in limited angle tomography. *Inverse Problems*. 2013;29(12):125007.
- [3] Canny J. A Computational Approach to Edge Detection. *IEEE Transactions on Pattern Analysis and Machine Intelligence*. 1986;PAMI-8(6):679–698.
- [4] Louis AK. Combining Image Reconstruction and Image Analysis with an Application to Two-Dimensional Tomography. *SIAM J Img Sci*. 2008;1:188–208.
- [5] Natterer F, Wübbeling F. Mathematical methods in image reconstruction. *SIAM Monographs on Mathematical Modeling and Computation*. Philadelphia, PA: Society for Industrial and Applied Mathematics (SIAM); 2001.
- [6] Candès EJ, Romberg JK, Tao T. Stable signal recovery from incomplete and inaccurate measurements. *Comm Pure Appl Math*. 2006;59(8):1207–1223.
- [7] Bubba TA, Hauptmann A, Huotari S, et al. Tomographic X-ray data of a lotus root filled with attenuating objects. 2016; p. 1–11. arXiv:1609.07299 [physics.data-an].
- [8] Daubechies I, Defrise M, De Mol C. An iterative thresholding algorithm for linear inverse problems with a sparsity constraint. *Comm Pure Appl Math*. 2004;57(11):1413–1457.